Constant-Amplitude 2π Phase Modulation from Topological Pole-Zero Winding

Alex Krasnok[*]

Department of Electrical and Computer Engineering, Florida International University, Miami, Florida 33174, USA and Knight Foundation School of Computing and Information Sciences, Florida International University, Miami, Florida 33174, USA

(Received 22 May 2025; revised 26 May 2026; accepted 1 June 2026; published 27 July 2026)

A resonant phase shifter should rotate a complex optical field without changing its magnitude, but loss and coupling usually make resonant phase tuning change the intensity as well. We introduce a pole-zero synthesis rule that produces a full 2π phase winding at a chosen scattering magnitude for a selected matrix element S_{ij}. The rule traces a closed iso-$|S_{ij}|$ contour that encloses a scattering zero and excludes the relevant pole; Cauchy's argument principle fixes the phase winding, and the contour fixes the amplitude. For a single isolated resonance, this contour is an Apollonius circle, giving a closed-form design. We realize the rule either by finite-time complex-frequency waveform excitation of a static resonator or by adiabatic comodulation of detuning with damping or coupling at a real carrier. We also discuss the extra control-dimensionality needed for simultaneous multichannel operation.

DOI: 10.1103/xt46-rfjs

Introduction—A phase shifter should rotate a complex field at fixed magnitude. This operation underlies coherent communication, interferometric metrology, phased arrays, beam steering, and programmable photonic processors [1–7]. Integrated photonics often uses resonators to reduce footprint, voltage, and energy per phase operation [1,4,8–11]. A lossy resonator, however, does not generally act as an all-pass element: tuning its resonance frequency, loss rate, or coupling rate changes both the optical phase and the scattering magnitude. This amplitude-phase comodulation, or amplitude modulation-phase modulation (AM-PM) conversion, complicates calibration and limits high-fidelity phase operations in compact circuits [12–14].

The limitation has a geometric origin. A linear time-invariant photonic network is described by a scattering matrix $\boldsymbol{S}(\tilde{f})$, where $\tilde{f}$ is complex frequency and S_{ij} maps an incoming wave in channel j to an outgoing wave in channel i. Poles of S_{ij} describe resonant buildup, and zeros describe destructive scattering. These poles and zeros are phase singularities: when a closed trajectory winds around a zero but not around a pole, the unwrapped phase changes by 2π according to Cauchy's argument principle [15–17]. This topological statement alone does not make a useful phase shifter because an arbitrary winding path generally changes the scattering amplitude.

This Letter turns pole-zero winding into a synthesis rule for amplitude-flat phase control. We choose a target scattering magnitude C and trace a closed iso-$|S_{ij}|$ contour that encloses a zero while excluding the associated pole. The phase winding is fixed by the enclosed singularities, whereas the magnitude is fixed by the selected contour. For a one-pole, one-zero resonant response, the isoamplitude contour is an Apollonius circle, so the required trajectory follows from geometry rather than numerical optimization. Figure 1 summarizes two implementations: Protocol (i) moves the excitation through complex frequency for a static resonator and Protocol (ii) moves the resonator pole-zero constellation around a fixed real carrier.

Selected-channel control differs from simultaneous multichannel control. A single scalar loop can make one channel S_{ij} amplitude flat. Simultaneous operation of several channels requires a loop in a higher-dimensional control space that satisfies several magnitude constraints at once. We give this matrix-level formulation below and state the corresponding degree-of-freedom requirement. This clarification separates the scalar building block from true multichannel operation in multiport resonators, interferometric meshes, and programmable photonic processors.

The construction connects standard complex analysis to practical resonant photonics. Non-Hermitian and topological photonics have shown that poles, zeros, exceptional points, and scattering singularities organize optical response in the complex-frequency plane [18–23]. Related ideas have been used in coherent absorption, virtual critical coupling, and metasurface phase engineering [24–29]. Here the new element is constructive: the isoamplitude condition selects the trajectory, and the enclosed pole-zero content selects the net phase. The result does not require unitary scattering, conventional all-pass operation, or interferometric amplitude equalization.

The protocols have clear operating limits. In Protocol (i), complex-frequency excitation means finite-time waveform synthesis: the real part f_R of $\tilde{f} = f_R + \mathrm{i} f_I$ sets the

[*]Contact author: akrasnok@fiu.edu

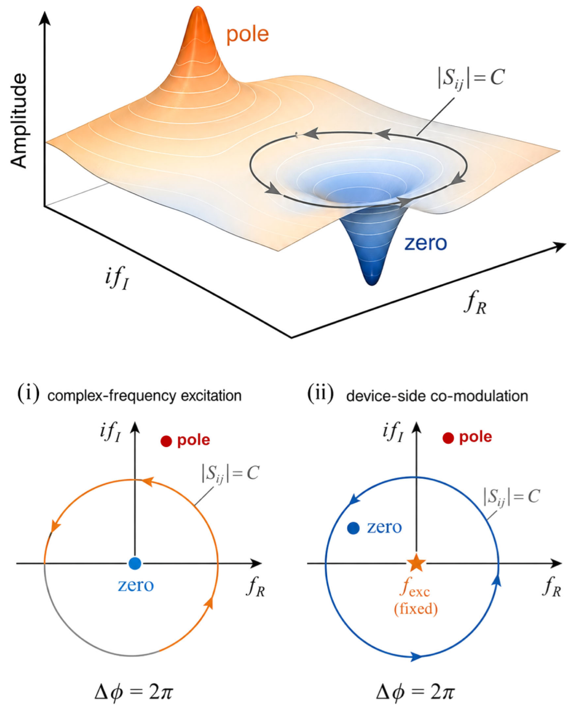

FIG. 1. Topological constant-amplitude phase control in the complex-frequency plane. A resonant scattering coefficient has a pole, where the response diverges in the analytic continuation, and a zero, where the selected scattering amplitude vanishes. A closed trajectory on an iso-$|S_{ij}|$ manifold accumulates a quantized phase when it encloses a net pole-zero charge. Protocol (i) uses a waveform-synthesized complex-frequency excitation to trace an isoamplitude loop around a static zero. Protocol (ii) comodulates device parameters so that a zero winds around a fixed real excitation while $|S_{ij}| = C$ remains constant.

instantaneous carrier frequency and the imaginary part f_I sets the exponential envelope through $e^{i2\pi\tilde{f}t} = e^{i2\pi f_R t}e^{-2\pi f_I t}$. In Protocol (ii), we assume adiabatic modulation, $\Omega_{\mathrm{mod}} \ll 2\pi(\Gamma_0 + \Gamma_c)$, where Ω_{mod} is the modulation angular frequency, Γ_0 is the intrinsic loss rate, and Γ_c is the external coupling rate. Under this condition, the scattering response follows the instantaneous pole-zero constellation; faster modulation produces Floquet sidebands and requires a time-varying scattering treatment [30].

Model and complex-plane structure—We model a linear, time-invariant, causal photonic network by its scattering matrix $\boldsymbol{S}(\tilde{f})$. With the convention $e^{+i2\pi\tilde{f}t}$, a stable causal response is analytic for $\mathrm{Im}\{\tilde{f}\} < 0$; stable resonant poles lie outside this causal half-plane. In open resonant systems, those poles coincide with quasinormal-mode frequencies, and reduced-order temporal coupled-mode theory (TCMT) describes the response with a small number of poles and zeros [31–34].

A single isolated resonance gives the minimal analytic form. When one resonance dominates a selected channel S_{ij} and the nonresonant background varies slowly over the linewidth, TCMT gives

$$S_{ij}(\tilde{f}) = S_{ij}^{\mathrm{bg}} \frac{\tilde{f} - \tilde{f}_{z,ij}}{\tilde{f} - \tilde{f}_p}. \tag{1}$$

Here S_{ij}^{bg} is the local background scattering coefficient, $\tilde{f}_{z,ij}$ is the zero of channel S_{ij}, and $\tilde{f}_p$ is the resonant pole. Equation (1) is local in frequency: if several resonances or a rapidly varying background contribute, the same winding statement applies to the full meromorphic response, but the single-circle Apollonius formula below no longer gives the complete contour.

The one-port resonator gives a closed-form example of the synthesis rule. We consider a single resonance with resonance frequency f_0, intrinsic loss rate $\Gamma_0 > 0$, and external coupling rate $\Gamma_c > 0$. In the complex-frequency plane, the reflection coefficient is

$$r(\tilde{f}) = \frac{i(\tilde{f} - f_0) + (\Gamma_0 - \Gamma_c)}{i(\tilde{f} - f_0) + (\Gamma_0 + \Gamma_c)}. \tag{2}$$

Equation (2) factorizes as the pole-zero ratio $r(\tilde{f}) = (\tilde{f} - \tilde{f}_z)/(\tilde{f} - \tilde{f}_p)$, with reflection zero $\tilde{f}_z = f_0 + i(\Gamma_0 - \Gamma_c)$ and pole $\tilde{f}_p = f_0 + i(\Gamma_0 + \Gamma_c)$. The zero reaches the real-frequency axis at critical coupling, $\Gamma_0 = \Gamma_c$, which is the standard condition for coherent perfect absorption in this one-channel setting [35].

The phase winding follows directly from the argument principle. For a closed contour $\mathcal{C}_f$ in the $\tilde{f}$-plane that does not cross a zero or pole of r,

$$\Delta\phi_{\mathcal{C}_f} = \mathrm{Im} \oint_{\mathcal{C}_f} d \ln r(\tilde{f}) = 2\pi(N_0 - N_p), \tag{3}$$

where N_0 and N_p are the numbers of enclosed zeros and poles, respectively, counted with multiplicity [15–17]. A counterclockwise loop around $\tilde{f}_z$ that excludes $\tilde{f}_p$ gives $\Delta\phi_{\mathcal{C}_f} = 2\pi$. A loop around $\tilde{f}_p$ that excludes $\tilde{f}_z$ gives -2π.

The constant-amplitude constraint selects the loop. Requiring $|r(\tilde{f})| = C$ is equivalent to the distance-ratio condition $|\tilde{f} - \tilde{f}_z| = C|\tilde{f} - \tilde{f}_p|$, which defines the Apollonius locus: the set of points with fixed distance ratio C to the two foci $\tilde{f}_z$ and $\tilde{f}_p$ [36]. For $C \neq 1$, this condition gives

$$(f_R - f_0)^2 + \left[f_I - \left(\Gamma_0 - \Gamma_c \frac{1 + C^2}{1 - C^2}\right)\right]^2 = \left(\frac{2C\Gamma_c}{|1 - C^2|}\right)^2. \tag{4}$$

For the zero-enclosing branch used for $+2\pi$ phase modulation in Eq. (2), the target magnitude satisfies $0 < C < 1$. In this range, the circle in Eq. (4) encloses $\tilde{f}_z$ and excludes $\tilde{f}_p$. For $C > 1$, the finite Apollonius circle encloses the pole instead and gives the opposite winding. For $C = 1$, the circle degenerates into the perpendicular bisector of the pole-zero segment.

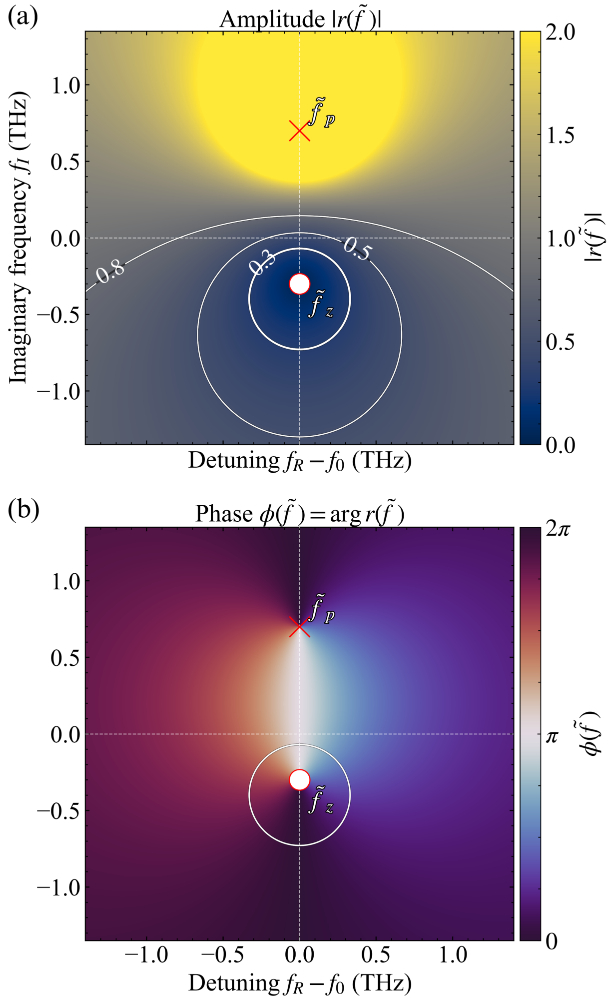

FIG. 2. Complex-frequency maps of the one-port reflection coefficient $r(\tilde{f})$ for $f_0 \simeq 193.41$ THz ($\lambda_0 \simeq 1.55$ μm), $\Gamma_0 = 0.2$ THz, and $\Gamma_c = 0.5$ THz. The horizontal axis is the detuning $f_R - f_0$. (a) Amplitude $|r(\tilde{f})|$. The zero $\tilde{f}_z = f_0 + \mathrm{i}(\Gamma_0 - \Gamma_c)$ and pole $\tilde{f}_p = f_0 + \mathrm{i}(\Gamma_0 + \Gamma_c)$ are marked by a circle and a cross, respectively. White curves show representative iso-$|r|$ Apollonius contours; the $|r| = 0.3$ loop is emphasized. (b) Phase $\phi(\tilde{f}) = \arg r(\tilde{f})$. The same $|r| = 0.3$ loop shows the constant-amplitude trajectory that winds around the zero while excluding the pole.

Equation (4) is the closed-form scalar synthesis rule. Choosing C fixes the loop radius and center; choosing the loop orientation fixes the sign of the phase winding. Figure 2 shows the amplitude and phase landscapes for the parameters used in the numerical examples. Points with $f_I \neq 0$ represent the analytic continuation of the response in the Laplace domain. They correspond to finite-time exponentially weighted excitations, not steady-state optical gain.

Approach 1: Complex-frequency excitation on an isoamplitude loop—A static resonator can realize the winding protocol when the source synthesizes the complex-frequency excitation. We keep the resonator parameters fixed: the resonance frequency is f_0, the intrinsic loss rate is Γ_0, and the external coupling rate is Γ_c. The incident waveform is programmed so that its instantaneous complex frequency, $\tilde{f}_{\mathrm{exc}}(t) = f_R(t) + \mathrm{i}f_I(t)$, samples the isoamplitude contour in the complex-frequency plane. A constant complex-frequency tone $e^{\mathrm{i}2\pi\tilde{f}t}$ is a carrier at f_R with envelope $e^{-2\pi f_I t}$; therefore $f_I > 0$ gives temporal decay and $f_I < 0$ gives temporal growth over the chosen time window. Optical arbitrary waveform generation and line-by-line pulse shaping provide the required control of instantaneous frequency and complex-envelope amplitude [37–40]. Segments with $f_I < 0$ require finite-duration execution and bounded dynamic range. This is the same physical setting as complex-frequency loading and virtual critical coupling, where tailored pulses emulate complex-frequency drives in integrated resonators [25,26].

The target magnitude selects the excitation loop. For the one-port response, choosing $0 < C < 1$ fixes the zero-enclosing iso-$|r|$ Apollonius contour given by Eq. (4). Driving $\tilde{f}_{\mathrm{exc}}(t)$ once around this contour encloses the reflection zero $\tilde{f}_z$ and excludes the pole $\tilde{f}_p$. Cauchy's argument principle then gives $\Delta\phi = 2\pi$, while the contour enforces $|r(\tilde{f}_{\mathrm{exc}})| = C$. Here "constant amplitude" means constant magnitude of the scattering coefficient, namely the ratio $|s_{\mathrm{out}}/s_{\mathrm{in}}|$. The reflected waveform still carries the programmed input envelope. A system that needs a flat output envelope can normalize by the known input envelope or use recombination in an interferometric or multiport architecture without changing the pole-zero winding.

Figure 3 shows why the complex-frequency loop is needed. A conventional real-frequency sweep with $f_I = 0$ produces strong AM-PM conversion and does not complete a clean 2π phase operation [Fig. 3(a)]. By contrast, the isoamplitude contour at $|r| = 0.3$ gives a full unwrapped 2π phase shift while keeping $|r|$ fixed within numerical tolerance [Fig. 3(b)]. The same scalar construction applies to a selected scattering element S_{ij} by replacing r with that channel response. It does not, by itself, control all outputs of a multiport device; simultaneous multichannel operation requires the additional constraints stated in the Discussion below. Details on finite-time complex-frequency excitation and dynamic range are given in Supplemental Material [41], Sec. S5.

Approach 2: Dynamic pole-zero motion around a fixed-frequency excitation—A device-side protocol can keep the optical source strictly monochromatic. We drive the resonator at a fixed real frequency f_{exc} and adiabatically move the instantaneous pole-zero constellation around that operating point. The adiabatic condition is $\Omega_{\mathrm{mod}} \ll 2\pi(\Gamma_0 + \Gamma_c)$, where Ω_{mod} is the modulation angular frequency. Under this condition, the carrier follows the instantaneous scattering coefficient. Faster modulation generates Floquet sidebands and requires a time-varying scattering treatment [30]. At fixed f_{exc}, the instantaneous reflection is $r(f_{\mathrm{exc}}, t) = [f_{\mathrm{exc}} - \tilde{f}_z(t)]/[f_{\mathrm{exc}} - \tilde{f}_p(t)]$,

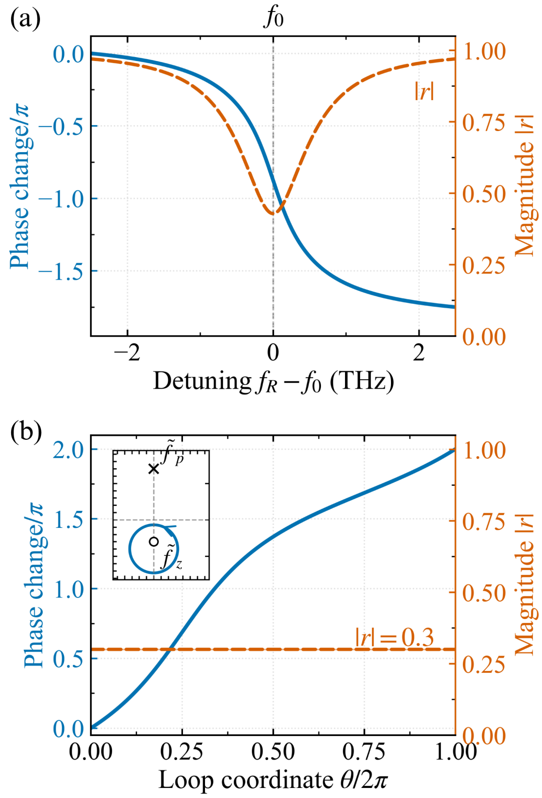

FIG. 3. Approach 1: source-side phase winding with a static resonator. (a) A conventional real-frequency sweep at $f_I = 0$ produces an incomplete phase excursion and strong amplitude variation. (b) A synthesized complex-frequency drive follows the zero-enclosing iso-$|r|$ Apollonius loop with $|r| = 0.3$, producing a full 2π phase change while keeping the scattering magnitude fixed. Inset: the loop in the complex-frequency plane; the trajectory encloses the reflection zero $\tilde{f}_z$ and excludes the pole $\tilde{f}_p$.

where $\tilde{f}_z(t) = f_0(t) + \mathrm{i}[\Gamma_0(t) - \Gamma_c]$ and $\tilde{f}_p(t) = f_0(t) + \mathrm{i}[\Gamma_0(t) + \Gamma_c]$. If $\tilde{f}_z(t)$ winds once counterclockwise around f_{exc} while $\tilde{f}_p(t)$ does not, the reflected phase accumulates $\Delta\phi = 2\pi$. We suppress AM-PM conversion by imposing $|r(f_{\mathrm{exc}}, t)| = C_d$ throughout the cycle, where C_d is the chosen device-side reflection magnitude.

Comodulating detuning and intrinsic damping gives a closed-form isoamplitude loop. We vary $f_0(t)$ and $\Gamma_0(t)$ while holding Γ_c fixed. The isoamplitude condition $|r(f_{\mathrm{exc}}, t)| = C_d$ forces (f_0, Γ_0) to trace a circle centered at $f_0 = f_{\mathrm{exc}}$ and $\Gamma_0 = \Gamma_{0,\mathrm{center}}$, where $\Gamma_{0,\mathrm{center}} = [(1 + C_d^2)/(1 - C_d^2)]\Gamma_c$. The radius is $R_{\mathrm{param}} = [2C_d/(1 - C_d^2)]\Gamma_c$ for $0 < C_d < 1$ (derivation in Supplemental Material [41], Sec. S4). This circle makes the zero and pole trace two equal-radius loops in the complex-frequency plane. Because the pole is shifted upward from the zero by $2\Gamma_c$, the fixed operating point lies inside the zero loop but outside the pole loop. Figure 4(a) shows this topology, and Fig. 4(b) confirms a 2π phase winding at constant $|r| = C_d$ within numerical tolerance.

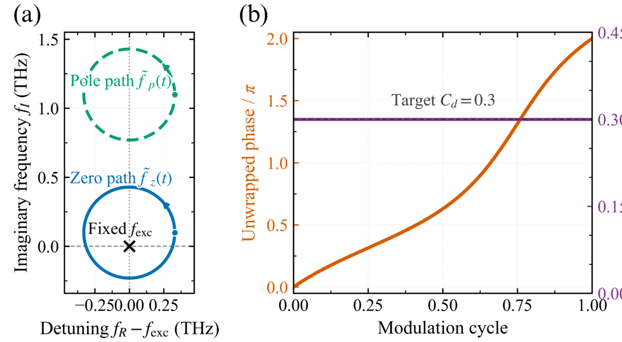

FIG. 4. Approach 2: device-side phase control at fixed real frequency. (a) The dynamically tuned zero $\tilde{f}_z(t)$ winds around the fixed excitation f_{exc}, whereas the pole $\tilde{f}_p(t)$ does not. (b) At f_{exc}, the reflected phase accumulates 2π over one modulation cycle while the scattering magnitude remains fixed at the target value C_d.

The numerical example in Fig. 4 sets the required modulation scale. For $C_d = 0.3$ and $\Gamma_c = 0.5$ THz, the radius is $R_{\mathrm{param}} = 0.329$ THz, the loss-loop center is $\Gamma_{0,\mathrm{center}} = 0.599$ THz, and the intrinsic loss spans $\Gamma_0 \in [0.269, 0.929]$ THz. The maximum resonance-frequency excursion is therefore 0.329 THz, which corresponds to a wavelength excursion of about 2.6 nm at $f_{\mathrm{exc}} \simeq 193.41$ THz, or $\lambda \simeq 1.55$ μm. This broad-linewidth choice makes the topology visible in the figure; it is not a fundamental requirement. Because all excursions scale linearly with Γ_c, a resonator with $\Gamma_c = 10$ GHz would require $R_{\mathrm{param}} = 6.6$ GHz, $\Gamma_0 \in [5.4, 18.6]$ GHz, and a wavelength excursion of 0.053 nm at 1.55 μm. Using $\Delta f_0/f_0 \simeq -\Delta n_{\mathrm{eff}}/n_g$ with $n_g \simeq 4$, this corresponds to $\Delta n_{\mathrm{eff}} \simeq 1.4 \times 10^{-4}$, i.e., an order-kelvin thermo-optic shift in silicon [42].

The practical bottleneck is synchronized loss or coupling control, not the resonance-frequency shift. The resonance frequency $f_0(t)$ can be tuned by thermo-optic, electro-optic, carrier-dispersion, or phase-change actuation. The effective damping can be tuned by controlled absorption, for example, through carrier-induced or graphene-assisted loss, or by coupling to an auxiliary dissipative channel [26,43]. A cleaner integrated route is to comodulate detuning and external coupling $\Gamma_c(t)$ instead of directly modulating intrinsic loss. Coupling-modulated silicon microrings have already demonstrated modulation beyond the conventional cavity-linewidth limit, which makes this route attractive for implementing the required pole-zero motion [44].

Reducing the target magnitude lowers the required tuning range but reduces signal. For $C_d \ll 1$, the radius scales as $R_{\mathrm{param}} \approx 2C_d\Gamma_c$, so operation closer to a scattering zero reduces the detuning, loss, or coupling excursion needed for a full 2π phase action (Supplemental Material [41], Sec. S8). The trade-off is lower raw output power and higher phase-noise sensitivity as $|r| \to 0$. Practical circuits can operate at small but finite C_d and recover usable output through interferometric recombination or multiport routing while preserving the zero-winding phase rule.

Discussion and outlook—The result is a synthesis rule, not a near-cancellation recipe. For a selected channel S_{ij}, choose a compatible target magnitude C, trace a closed iso-$|S_{ij}|$ manifold, enclose the relevant scattering zero, and exclude the relevant pole. The net phase winding is then fixed by $\Delta\phi = 2\pi(N_0 - N_p)$, whereas amplitude flatness comes from tracking the selected isoamplitude contour. In the one-pole, one-zero branch used above, zero-enclosing $+2\pi$ operation corresponds to $0 < C < 1$; choosing $C > 1$ selects the pole-enclosing branch and reverses the winding sign.

True simultaneous multichannel operation requires more than a scalar replacement $r \to S_{ij}$. Let $\mathcal{M} = \{(i_\mu, j_\mu)\}_{\mu=1}^{K}$ denote K scattering channels to be controlled at the same operating excitation, and let $\boldsymbol{\lambda} \in \mathbb{R}^d$ collect the available real controls, such as detuning, intrinsic loss, and external coupling rates. A simultaneous amplitude-flat loop must satisfy $|S^{\mathrm{op}}_{i_\mu j_\mu}[\boldsymbol{\lambda}(t)]| = C_\mu$ for every $\mu = 1, \ldots, K$. The summed phase is the winding of the product $G^{\mathrm{op}}_{\mathcal{M}} = \prod_{\mu=1}^{K} S^{\mathrm{op}}_{i_\mu j_\mu}$, so $\Delta\Phi_{\mathcal{M}} = \Delta \arg G^{\mathrm{op}}_{\mathcal{M}}$ and, when the product is meromorphic in the loop variable, $\Delta\Phi_{\mathcal{M}} = 2\pi(N_0^G - N_p^G)$. Generically, the K magnitude constraints leave a $(d-K)$-dimensional manifold, so a closed loop requires $d \geq K + 1$. Symmetry can reduce this count, but absent such structure, simultaneous multichannel phase control needs additional tunable parameters beyond a single scalar complex-frequency loop. The scalar construction above is the $K = 1$ building block; true simultaneous control of several channels needs additional controls or symmetry-protected degeneracies.

The two protocols distribute complexity differently. Approach 1 keeps the device fixed and moves the control burden to the source. It is compatible with optical arbitrary waveform generation, line-by-line pulse shaping, and finite-time complex-frequency loading [25,26,37,38]. Its main constraints are dynamic range and finite-window transients, especially on loop segments with $f_I < 0$. Approach 2 keeps the drive monochromatic and moves the burden to the device. It is compatible with resonant integrated platforms that can comodulate detuning, damping, or external coupling; its main constraints are adiabaticity and synchronized parameter control.

The topology protects the integer phase winding, not every experimental imperfection. Smooth loop deformations leave $\Delta\phi = 2\pi(N_0 - N_p)$ unchanged as long as the loop does not cross a pole or zero. Amplitude flatness, however, depends on how accurately the device or source tracks the iso-$|S_{ij}|$ manifold. Nonadiabatic modulation adds Floquet sidebands and breaks the instantaneous-response approximation; this regime requires a time-varying scattering treatment [30]. Operating near a zero reduces the required tuning excursion, but it also lowers the signal and increases phase-noise sensitivity. These trade-offs set the design point rather than the validity of the pole-zero synthesis rule.

Conclusions—We showed that full-range resonant phase control can be designed as an isoamplitude pole-zero winding. The prescription is explicit: choose a scattering channel S_{ij}, choose a compatible constant magnitude, close the loop around a zero, and avoid pole encirclement. Cauchy's argument principle fixes the net phase to $2\pi(N_0 - N_p)$, and the isoamplitude constraint suppresses AM-PM conversion.

The one-resonance case gives a closed-form design and a concrete implementation scale. Complex-frequency excitation realizes the loop with a static resonator and a shaped incident waveform. Device-side tuning realizes the same topology at a fixed real carrier by comodulating detuning and loss or coupling. For the example $C_d = 0.3$ and $\Gamma_c = 0.5$ THz, the required parameter-space radius is 0.329 THz; for $\Gamma_c = 10$ GHz, the same dimensionless protocol requires a 6.6 GHz resonance shift, corresponding to $\Delta n_{\mathrm{eff}} \simeq 1.4 \times 10^{-4}$ for $n_g \simeq 4$.

The scalar channel result is the building block for multiport photonics. Simultaneous multichannel operation requires a higher-dimensional control loop that satisfies several isoamplitude constraints at once. This distinction matters for resonant routers, interferometric meshes, programmable photonic processors, and quantum photonic circuits, where phase operations must remain amplitude flat across selected outputs rather than in a single monitored channel.

Acknowledgments—The author acknowledges financial support from the U.S. Department of Energy (DoE) and the U.S. Air Force Office of Scientific Research (AFOSR).

Data availability—The numerical data and plotting scripts used to generate Figs. 2–4 are available from the author upon reasonable request.

[1] J. Parra, J. Navarro-Arenas, and P. Sanchis, Adv. Photonics Nexus **3**, 044001 (2024).
[2] T. Xu, Y. Dong, Q. Zhong, S. Zheng, Y. Qiu, X. Zhao, L. Jia, C. Lee, and T. Hu, Nanophotonics **12**, 3683 (2023).
[3] T. Kawanishi, *Electro-Optic Modulation for Photonic Networks: Precise and High-Speed Control of Lightwaves* (Springer, Cham, 2022).
[4] A. Rahim, A. Hermans, B. Wohlfeil, D. Petousi, B. Kuyken, D. Van Thourhout, and R. Baets, Adv. Photonics **3**, 024003 (2021).
[5] M. Xu *et al.*, Nat. Commun. **11**, 3911 (2020).
[6] I. C. Reines, M. G. Wood, T. S. Luk, D. K. Serkland, and S. Campione, Opt. Express **26**, 21594 (2018).
[7] C. Dong *et al.*, Nanoscale Horiz. **10**, 933 (2025).
[8] H. Sun, Q. Qiao, Q. Guan, and G. Zhou, Micromachines **13**, 1509 (2022).
[9] P. Prabhathan *et al.*, iScience **26**, 107946 (2023).

[10] N. C. Harris, Y. Ma, J. Mower, T. Baehr-Jones, D. Englund, M. Hochberg, and C. Galland, Opt. Express **22**, 10487 (2014).

[11] J. Y. Kim, J. Park, G. R. Holdman, J. T. Heiden, S. Kim, V. W. Brar, and M. S. Jang, Nat. Commun. **13**, 2103 (2022).

[12] J. A. Taylor, F. Quinlan, A. Hati, C. Nelson, S. A. Diddams, S. Datta, and A. Joshi, in *2010 IEEE International Frequency Control Symposium* (IEEE, Newport Beach, CA, 2010), pp. 684–688.

[13] Z. Tai, L. Yan, Y. Zhang, X. Zhang, W. Guo, S. Zhang, and H. Jiang, Opt. Lett. **41**, 5584 (2016).

[14] P. S. Kincaid, N. Andriolli, G. Contestabile, and L. De Marinis, Commun Eng. **4**, 58 (2025).

[15] L. V. Ahlfors, *Complex Analysis: An Introduction to the Theory of Analytic Functions of One Complex Variable*, 3rd ed. (American Mathematical Society, Providence, RI, 2021).

[16] W. Li and L. C. Paulson, in *Interactive Theorem Proving*, edited by J. C. Blanchette and S. Merz (Springer International Publishing, Cham, 2016), Vol. 9807, pp. 235–251.

[17] J. M. Howie, *Complex Analysis*, 2nd printing ed. (Springer, London, 2004).

[18] Y. Ashida, Z. Gong, and M. Ueda, Adv. Phys. **69**, 249 (2020).

[19] C. M. M. Bender, Rep. Prog. Phys. **70**, 947 (2007).

[20] E. J. Bergholtz, J. C. Budich, and F. K. Kunst, Rev. Mod. Phys. **93**, 015005 (2021).

[21] L. Feng, R. El-Ganainy, and L. Ge, Nat. Photonics **11**, 752 (2017).

[22] M.-A. Miri and A. Alù, Science **363**, eaar7709 (2019).

[23] Z. Gong, Y. Ashida, K. Kawabata, K. Takasan, S. Higashikawa, and M. Ueda, Phys. Rev. X **8**, 031079 (2018).

[24] Z. Sakotic, A. Krasnok, A. Alù, and N. Jankovic, Photonics Res. **9**, 1310 (2021).

[25] Y. Ra'di, A. Krasnok, and A. Alù, ACS Photonics **7**, 1468 (2020).

[26] J. Hinney, S. Kim, G. J. K. Flatt, I. Datta, A. Alù, and M. Lipson, Nat. Commun. **15**, 2741 (2024).

[27] S. Kim, A. Krasnok, and A. Alù, Science **387**, eado4128 (2025).

[28] A. Krasnok, D. Baranov, H. Li, M.-A. Miri, F. Monticone, and A. Alù, Adv. Opt. Photonics **11**, 892 (2019).

[29] R. Colom, E. Mikheeva, K. Achouri, J. Zuniga-Perez, N. Bonod, O. J. F. Martin, S. Burger, and P. Genevet, Laser Photonics Rev. **17**, 2200976 (2023).

[30] E. Galiffi, R. Tirole, S. Yin, H. Li, S. Vezzoli, P. A. Huidobro, M. G. Silveirinha, A. Alù, and J. B. Pendry, Adv. Opt. Photonics **4**, 014002 (2022).

[31] F. Alpeggiani, N. Parappurath, E. Verhagen, and L. Kuipers, Phys. Rev. X **7**, 021035 (2017).

[32] S. Fan, W. Suh, and J. D. Joannopoulos, J. Opt. Soc. Am. A **20**, 569 (2003).

[33] W. Suh, Z. Wang, and S. Fan, IEEE J. Quantum Electron. **40**, 1511 (2004).

[34] H. A. Haus and W. Huang, Proc. IEEE **79**, 1505 (1991).

[35] Y. D. Chong, L. Ge, H. Cao, and A. D. Stone, Phys. Rev. Lett. **105**, 053901 (2010).

[36] T. Needham, *Visual Complex Analysis* (Oxford University Press, Oxford, 1997).

[37] S. T. Cundiff and A. M. Weiner, Nat. Photonics **4**, 760 (2010).

[38] A. M. Weiner, Opt. Commun. **284**, 3669 (2011).

[39] C.-B. Huang, Z. Jiang, D. E. Leaird, J. Caraquitena, and A. M. Weiner, Laser Photonics Rev. **2**, 227 (2008).

[40] Z. Jiang, D. E. Leaird, and A. M. Weiner, Opt. Express **13**, 10431 (2005).

[41] See Supplemental Material at http://link.aps.org/supplemental/10.1103/xt46-rfjs for temporal coupled-mode derivations, isoamplitude contour derivations, waveform requirements, adiabaticity, robustness, tuning-scale estimates, and numerical details, which includes Ref. [34].

[42] J. Komma, C. Schwarz, G. Hofmann, D. Heinert, and R. Nawrodt, Appl. Phys. Lett. **101**, 041905 (2012).

[43] Y. Ding, X. Zhu, S. Xiao, H. Hu, L. H. Frandsen, N. A. Mortensen, and K. Yvind, Nano Lett. **15**, 4393 (2015).

[44] W. D. Sacher, W. M. J. Green, S. Assefa, T. Barwicz, H. Pan, S. M. Shank, Y. A. Vlasov, and J. K. S. Poon, Opt. Express **21**, 9722 (2013).